STRUCTURE DESIGN AND EVALUATION OF MOBILE PHONE SCREEN PROTECTOR APPLICATION MACHINE ORIENTED TOWARDS PERFORMANCE IMPROVEMENT

Yao-nan LI[1,2],Hao-tian Jin[2],Hao LIU[2],De-lun WANG[1],Bo ZHANG[2,*],Yi-hui WEN[2]

Presently, most mobile phone screen protector application in the market is manual, leading to low efficiency. A fully automatic device is designed. Its working principle, enabling process actions like screen protector positioning and adhesion, is detailed. Each component undergoes design modeling, balancing functional needs and structural rationality. Materials are selected based on component stress and working conditions. Strength and stiffness checks, along with optimization, are performed on key components for stable, reliable operation. Prototype fabrication and practical tests show the device surpasses manual operation in productivity and qualification rate, offering a reference for mass production.

Keywords: Mobile phone screen protector application machine; Structural design; Structural verification and optimization; Prototype experiment.

1. Introduction

Currently, the demand for mobile phone screen protector installation services is robust, yet the operation remains highly reliant on manual labor. Manual installation imposes stringent requirements on the skills and experience of operators, and is time-consuming and inefficient. In large-scale or high-demand scenarios, the limitations of manual installation become particularly evident, making it difficult to meet the demand for rapid and efficient services[1]. This not only affects user experience but also constrains the industry's efficiency improvement and scalability. Furthermore, the lack of widely available, highly efficient automated devices capable of replacing manual labor in the market underscores the urgent need for the development of such equipment[2]. Therefore, the development of automated, standardized, and efficient mobile phone screen protector installation devices to replace manual operations is of great significance for meeting market demands and driving industry advancement.

[1]School of Mechanical Engineering, Dalian University of Technology, Dalian,116000,China.
[2]School of Mechanical Engineering, Ningxia University, Yinchuan,750000,China.
* Corresponding author e-mail: zhangb@nxu.edu.cn

2. Process Motions and Parameters

(1) Clamping the Smartphone and Tempered Glass: The workstation prepares the smartphone for screen protector application and secures both the smartphone and tempered glass in place using its clamping mechanism[3].

(2) Positioning the Tempered Glass[4]: Position sensors in the control unit ensure precise alignment of the tempered glass with the smartphone screen for proper adhesion.

(3) Screen Cleaning: The cleaning mechanism removes contaminants from the screen using nozzles, wiping blocks, adhesive rollers, or similar devices to ensure optimal adhesion.

(4) Picking and Placing the Tempered Glass: A robotic arm retrieves the tempered glass from storage and positions it accurately on the smartphone.

(5) Applying Screen Protectors: Once aligned, the execution mechanism applies the screen protector uniformly, eliminating air bubbles[5].

(6) Check and Finish: After application, the machine stops, and the applied screen protector is inspected for quality compliance.

The productivity exceeds 100 units per hour per person and the qualification rate is over 90%[6].

3. Structure Design

3.1 Prime Mover

The prime mover, typically an electric motor, serves as the initial power source driving the entire mechanical system. It converts electrical energy into mechanical energy, supplying power to the system. The motor connects to the transmission mechanism (e.g., gears, racks) to deliver power to the execution mechanism, as illustrated in Fig. 1.

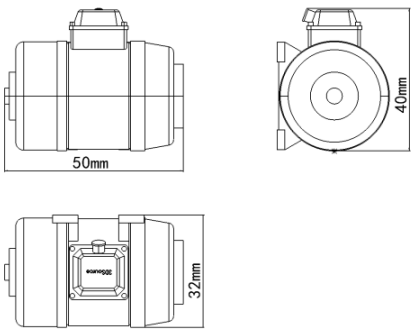

Fig. 1. Electric Motor

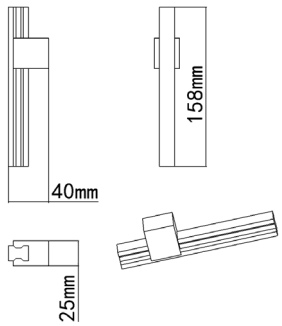

Fig. 2. Rails and Sliders

3.2 Transmission Mechanism

The transmission mechanism transfers power from the prime mover to the execution mechanism, enabling mechanical motion.

Rails and Sliders: These components work together to allow movement along specific directions. Rails are mounted on the baseplate and frame, while sliders move along the rails to position and transport wiping modules and screen protectors, as shown in Fig. 2.

Gears and Racks: Integrated with the X, Y, and Z-axis drive motors, these mechanisms convert rotational energy into precise linear motion. They enable smooth movement of sliders and beams along the X-axis, sliders and columns along the Y-axis, and columns along the Z-axis, ensuring accurate positioning and manipulation in a 3D coordinate system, as shown in Fig. 3.

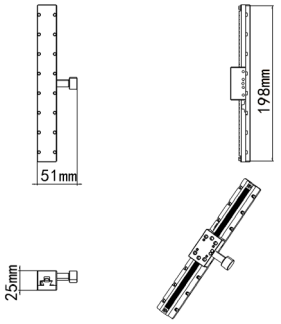

Fig. 3. Gears and Racks

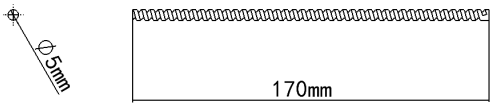

Fig. 4. Screw Components

Screw Components: Connected to motors, they transmit power to sliders through rotation, adjusting height in the Z-coordinate direction and moving back and forth in the Y-coordinate direction, as shown in Fig.4.

3.3 Execution Mechanism

The execution mechanism is the part of the mechanical system that directly completes the task, as shown in Fig.5.

Robotic arm: It consists of XYZ-axis guide rails and sliders to achieve precise spatial positioning.

Among them,

X-axis drive motor: Controls the movement in the X-axis direction.

Y-axis drive motor: Controls the movement in the Y-axis direction.

Z-axis drive motor: Controls the movement in the Z-axis direction.

Suction cup motor: Controls the suction power of the vacuum suction cup.

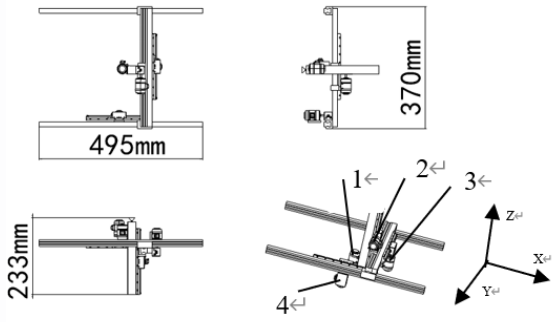

Fig. 5. Robotic Arm（1- Suction cup motor，
2- Z-axis drive motor，3- Y-axis drive motor，
4- X-axis drive motor）

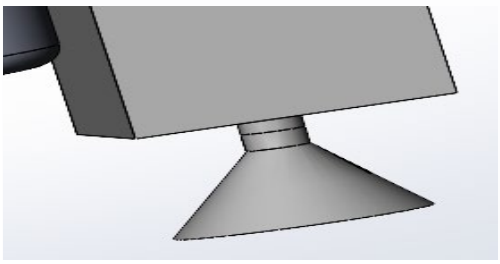

Fig. 6. Vacuum Suction Cup

Vacuum Suction Cup: Installed beneath the column of the robotic arm, it is used for picking up and placing mobile phone screens, as shown in Fig.6.

Wiping Mechanism: Comprising a wiping module and a motion module, it is responsible for cleaning the mobile phone screens, as shown in Fig.7.

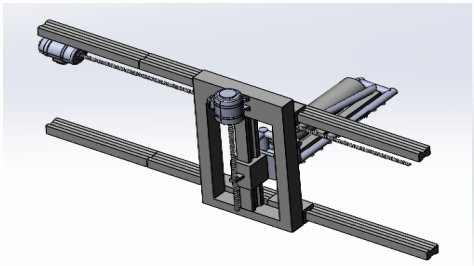

Fig. 7. Wiping Mechanism

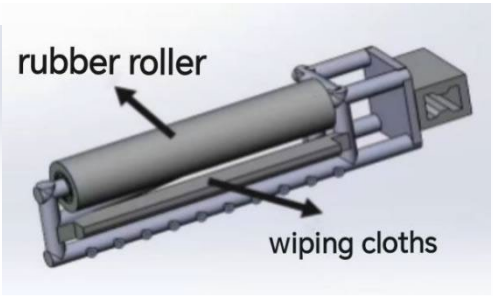

Fig. 8. Wiping Module

(1)Wiping Module: Composed of nozzles, wiping blocks, wiping cloths, rubber rollers, etc., it achieves screen cleaning. As shown in Fig.8.

(2)Motion Module: Comprising motors, screw assemblies, sliders, guide rails, etc., it is responsible for implementing the path movement of the wiping module, as shown in Fig.9.

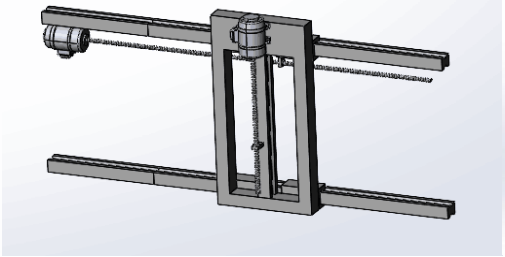

Fig. 9. Motion Module

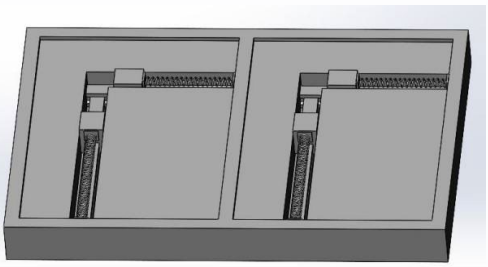

Fig. 10. Base Plate

Base Plate: Including a workbench, springs, guide rails, and sliders, it is used to fix mobile phones and phone screens and to achieve precise position adjustment, as shown in Fig.10.

3.4 General Assembly Drawing

Based on the analysis of the components of the prime movers, transmission mechanisms, and execution mechanisms, further integration and assembly can be performed to obtain the overall assembly diagram of the screen protector application machine, as shown in Fig.11.

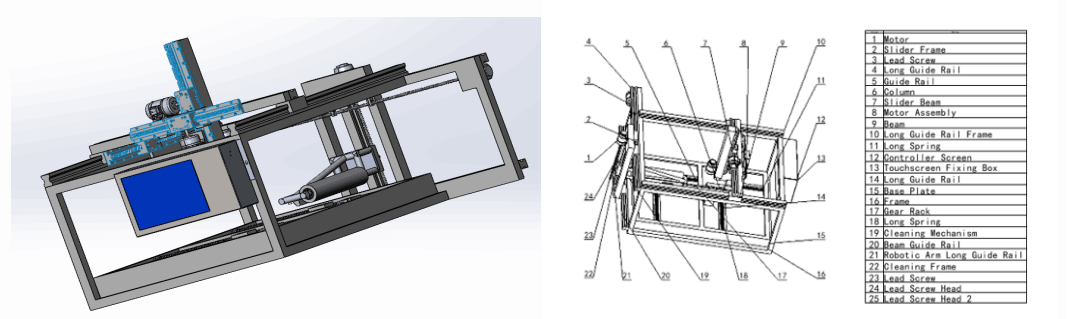

Fig. 11. General Assembly Diagram

4.Equipment Operating Condition Simulation and Analysis Optimization

Strength reflects the load-bearing capacity of the film applicator, ensuring structural integrity and normal operation under load; stiffness reflects the degree of deformation under external forces, ensuring that deformations remain within acceptable limits. Through strength and stiffness verification, design or manufacturing defects can be identified early, enabling targeted optimization to enhance equipment performance and extend service life.

4.1 Strength Verification and Optimization of the Base Plate

To ensure the base plate can withstand operational loads without damage while enabling further structural optimization, strength verification is conducted using Workbench software.

Safety Factor: A conservative safety factor of is adopted f_s=2, which is suitable for automated equipment.

Working Load:The weight of different mobile phones is generally within 200g. The weight of screen protectors can also vary slightly due to different thicknesses and materials, but the differences are generally insignificant.

Typically, screen protectors are relatively lightweight and we can assume an average weight of 10g[7].

Table 1

Weights of Different Mobile Phone Models

Model	Release Year	Weight
iPhone 12	2020	162g
iPhone 12 mini	2020	133g
Samsung Galaxy S24	2024	167g
Samsung Galaxy Note 10	2019	168g
Sony Xperia 10 IV	2022	161g
Huawei nova 12 Vitality Edition	2023	168g
OPPO Reno4 SE	2020	169g
Meizu 18	2021	162g
Realme X7 Pro Supreme Edition	2021	170g

Note: Data sourced from the official websites of respective mobile phone brands.

Table 2

The weights of different models of tablet computers

Model	Size	Weight
Apple iPad (2021)	10.2”	498g
Apple iPad Air (2022)	10.9”	462g
Samsung Galaxy Tab A9	8.7”	332g
Lenovo Tab M9	9”	344g
Huawei MatePad 11 (2023)	11”	480g
Xiaomi Redmi Pad Pro 5G	12.1”	566g
Vivo Pad 2 Pro	13”	679g

Since 1 kilogram (kg) equals 1000 grams (g), and the gravitational acceleration on Earth is approximately 9.81 m/s² , there will be a pressing force of around 5N during the application of the screen protector, ensuring a tight fit between the protector and the phone screen. Therefore, the theoretical maximum working load is approximately:

$$F=G+F'=[(1000+10)\div 1000]kg\times 9.81\,{}^{m}/_{s^2}+5N\approx 15.1N \quad (1)$$

Considering the safety factor, slightly increase this value, and the calculated working load is approximately:

$$F_s=f_s\times F=2\times 15.1\approx 30N \quad (2)$$

Strength Verification

(1) Model Parameter Determination[8]:
Material: Standard carbon steel (0.06–0.22% carbon content)
Elastic modulus: 206.8 GPa
Yield strength: 250 MPa

Component dimensions:Thickness: t=45mm, length: L=300mm, and width of the base plate: W=210mm.

(2) 3D Model Development: CAD software can be used for modeling. The model can be imported into Workbench for analysis or created directly using Workbench's built-in modules. In this study, SolidWorks was used to develop the 3D model, as shown in Figure 12.

(3) Finite Element Model Generation: The base plate is made of structural steel, with an elastic modulus of 206.8 GPa and a yield strength of 250 MPa.

The base plate undergoes mesh division, initially automated by Workbench but refined for better results. Dominated by regular tetrahedrons, the mesh uses a 10mm cell size for most regions, ensuring computational accuracy. To enhance precision in stress-concentrated areas of interest, a finer 5mm cell size is applied, balancing accuracy and computational efficiency.The resulting mesh is shown in Figure 13.

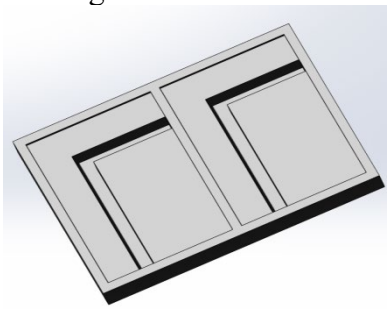

Fig. 12. The 3D Model of The Base Plate

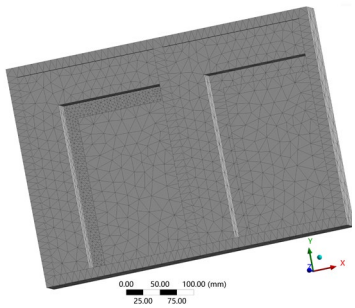

Fig. 13. Base Plate Mesh Diagram

(4)Static Stress Analysis: Fixed support is applied to the lower surface of the base plate (Fig. 14), and force is applied to the upper surface where the mobile phone or tablet is mounted (Fig. 15). The analysis yields a maximum total deformation of approximately (Fig. 16) and a maximum stress of 0.0009 MPa (Fig. 17).

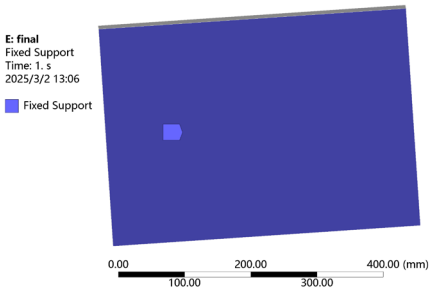

Fig. 14. Base Plate Support Diagram

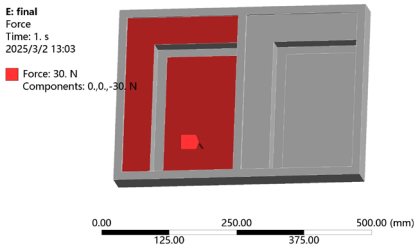

Fig. 15. Base Plate Load Diagram

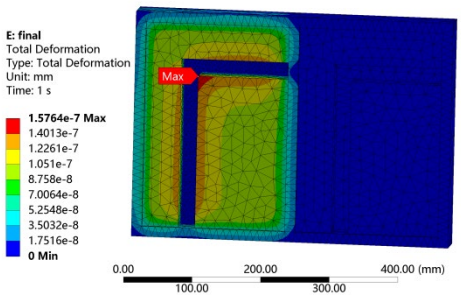

Fig. 16. Base Plate Deformation Diagram

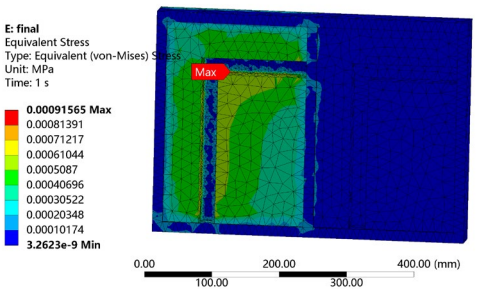

Fig. 17. Base Plate Static Stress Diagram

4.2 Optimization

Based on previous calculations, the maximum stress is significantly below the material's yield strength, meeting strength requirements. The overall deformation is negligible, satisfying stiffness criteria. To optimize the bottom plate for production cost and lightweight design, the following points can be considered:

(1) Material Selection[5]:

Table 3

Comparison of Material Properties

Material	Density	Strength	Elastic Modulus
Ordinary Carbon Steel	7.85g/cm³	200-500MPa	190-210GPa
Aluminum Alloy	2.63-2.85g/cm³	110-650MPa	68.9-73.1GPa
Carbon Fiber Reinforced Plastic(CFRP)	1.50-1.60g/cm³	Up to 600MPa and above	230-340GPa

Consider using aluminum alloy or carbon fiber reinforced plastic (CFRP) to replace traditional steel, reducing weight while maintaining strength.

(2) Structural Optimization: Under given load conditions, topology optimization (Fig. 18) is applied to determine the optimal material distribution, reducing material usage.Set an optimization condition to reduce the mass by 30% and optimize the baseplate.Reduce the thickness of the baseplate by 10 mm (refer to Figure 19).

Since the stress borne by the baseplate is significantly lower than the material's yield strength and the deformation is extremely small, a hollow or porous structural design can be adopted to further reduce the weight of this component. The three pairs of holes have diameters of 30 mm, 60 mm, and 90 mm, respectively (refer to Figure 20). When the same constraints and loads are applied to the modified model, simulation calculations indicate that, compared to the pre-optimization state, the changes in deformation and stress after optimization are not significant, and the impact on the material is negligible. Therefore, the design meets the requirements.

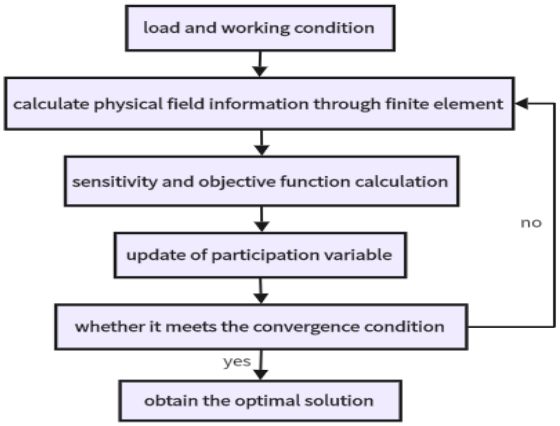

Fig. 18. Topology Optimization Design Process

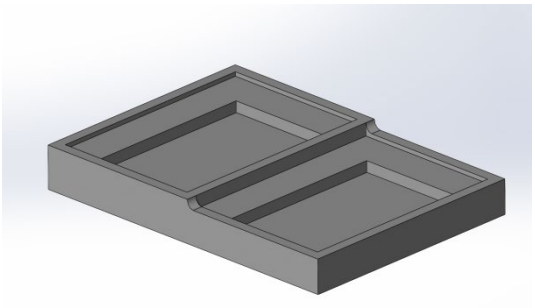

Fig. 19. Topology Optimization Improved Model

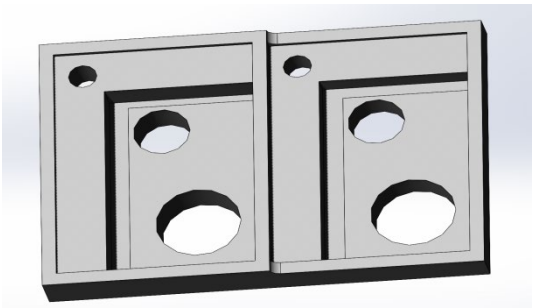

Fig. 20. Schematic Diagram of Structural Optimization

(3) Lightweight Design: Reassess and optimize component sizes to minimize material usage while meeting functional requirements, reducing the product's overall weight.

(4) Connection Methods: Welding or bonding offers lighter connections compared to traditional bolting, eliminating the need for additional fasteners. These methods also provide better sealing and enhanced overall performance.

4.3 Stiffness Verification

Since the robotic arm is used for the suction and transport of phone films, the deformation of the crossbeam connected to it directly affects the accuracy of the film application. Therefore, the deformation of the robotic arm’s crossbeam is the most critical aspect to focus on in the entire mechanical structure.

Material: Ordinary carbon steel (carbon content approximately 0.06~0.22%), with its elastic modulus $E = 206.8\text{GPa}$ and yield strength $f_u = 250\text{MPa}$.

Component dimensions: Length: $L_{beam} = 360mm$, width: $b = 15mm$, and height: $h = 20mm$ of the robotic arm crossbeam.

Load analysis[9]: For the robotic arm crossbeam, the main force application point is at the centroid of the crossbeam. The maximum force is primarily due to the film pressing force F'=5N. Taking into account other mechanical structures (such as servo motors and other accessories), the estimated operating load F is set as 15 N.Additionally, due to the safety factor $f_s = 2$, the working load can be obtained from Equation (4).

$$F_s = f_s \cdot F \tag{4}$$

The bending deformation of the crossbeam is calculated according to Equation (5).

$$\delta_{\max} = \frac{P \times L_{beam}^3}{48 \times E \times I} \tag{5}$$

Where the sectional moment of inertia I is calculated as:

$$I = \frac{b \times h^3}{12} \tag{6}$$

In the above equations,$\delta_{\max}$ is the maximum deflection (mm); P is the concentrated load (N); L_{beam} is the span of the mechanical arm beam (mm); E is the elastic modulus of the material (GPa); I is the moment of inertia of the beam section (mm^4); b is the width of the mechanical arm beam (mm); h is the height of the mechanical arm beam (mm).

By substituting $P=F_s$, I, and E=206.8GPa=206800N/mm^2 into Equation (5), the theoretical maximum deflection of the crossbeam is obtained, which is far smaller than 1 mm and can be considered negligible. Although the magnitude is so small that it exceeds the effective precision of practical engineering calculations, the result indicates that the stiffness of the crossbeam meets the design requirements [8]. It should be noted that this theoretical result does not account for factors such as joint looseness, assembly errors, and the actual distribution of loads, and is mainly used for a qualitative assessment of stiffness safety margins.

4.4. Motor Selection

4.4.1 Selection of Robotic Arm Motors

To meet the design requirements of the automatic film-applying machine in terms of precision (positioning accuracy $\leqslant$ 0.01 mm) and dynamic response (acceleration time $\leqslant$ 0.1 s), a servo motor should be selected as the motor type[9]. The mechanical arm beam with the heaviest load should be chosen for specific motor selection.

Total Load: 4 kg (including the beam and attached components)

Required Travel Distance: 495 mm in 5 seconds, resulting in a velocity of 99 mm/s

Pre-selected Gear Specifications: Module 2, gear teeth 17, pitch radius 34 mm

Calculated Torque and Speed:

Load force:

$$F = \mu mg + ma = 0.3 \times 4 \times 9.8 + 4 \times 0.1 = 12.16N \quad (6)$$

Torque:

$$T = \frac{Fd}{2} = \frac{12.16 \times 34}{2} = 206.72\ N \cdot mm \quad (7)$$

Speed:

$$n = \frac{99}{106.76} \times 60 = 55.64\ r/min \quad (8)$$

After evaluation, the GA12-N20 motor[10] (100 rpm, 215.6 N·mm torque) is selected for its suitability.

4.4.2 Selection of Pneumatic Motor

The suction cup has a diameter of d = 20 mm and a height of h = 10 mm, resulting in a volume (equivalent to a cylinder)of:

$$V = \pi \left(\frac{d}{2}\right)^2 h = 3.14 \times 100 \times 10 = 3140\ mm^3 \quad (9)$$

Including the pipeline and other components, the total volume is estimated to be 0.00005 m³. Assuming a vacuum extraction time of 0.5s, the required flow rate is calculated as follows:

$$Q = \frac{V}{t} = \frac{0.00005}{0.5} = 0.0001\ m^3/s \quad (10)$$

Given a vacuum pump suction pressure of 0.05 MPa, the pump power is determined as:

$$P = Q \cdot \Delta P = 0.0001 \times 0.05 \times 10^6 = 5\ W \quad (11)$$

Based on these calculations, the 2TNRK6GN-C motor[11] with a rated output of 6W is selected.

5. Mechanism of Adaptive Grasping and Positioning Control for Multi-Size Screen Protectors

The control unit of the mobile phone film-applying machine comprises an upper computer (industrial PC), a PLC (Siemens S7-1200), a central processing unit (ARM Cortex-A9), memory, and a servo controller. For different size categories of film-applying objects, differentiated control rules are formulated through sensors and a fuzzy PID algorithm to ensure that the vacuum suction cup accurately positions the center of the tempered glass film at the center of the

electronic product, enabling the grasping and positioning of multi-size screen protectors. The process is as follows:

(1) Center Position Calculation: The displacement of the slider is detected in real-time by position sensors, and the central processing unit calculates the center positions of both the electronic product and the tempered glass film.

(2) Multi-Size Screen Protector Grasping and Positioning Using an Elastic and Expandable Single Suction Cup Structure:

A bellow-type suction cup made of silicone material is employed, incorporating a pneumatic support structure inside[12]. The suction cup diameter can be automatically adjusted through negative pressure. When adhering to small-sized screens, the suction cup contracts to its minimum diameter (e.g., 15 mm); when adhering to large-sized screens, it expands to its maximum diameter (e.g., 30 mm), ensuring uniform distribution of suction force. Pressure sensors continuously monitor the vacuum level between the suction cup and the screen, and the system automatically adjusts the air pump output pressure accordingly. For example:

Small-sized screens (<6 inches): The vacuum level is set to -0.04 MPa to prevent excessive suction that could deform the screen.

Large-sized screens (⩾6 inches): The vacuum level is increased to -0.06 MPa to ensure sufficient suction.

(3) Multi-Size Screen Recognition & Data Transmission: A high-resolution CMOS camera at the workbench edge, coupled with OpenCV algorithms, identifies screen contours. The system measures the screen diagonal length in under 1 second via edge detection and size matching, automatically matching the model in a pre-stored library (e.g., iPhone 14 Pro Max, Galaxy S23 Ultra).

The memory holds parameters for over 200 mobile phone models (screen size, center offset, suction cup expansion, etc.). Upon screen recognition, the system fetches corresponding parameters, adjusting slider stroke, suction cup vacuum, and fuzzy PID rules. The CPU sends position data to the upper computer for processing and control instruction dispatch.

(4) Positioning Execution: The fuzzy PID algorithm runs on the upper computer, comparing the center positions of the vacuum suction cup, the tempered glass film, and the electronic product, and calculating the adjustment displacement. Control parameters are automatically adjusted based on displacement data and fuzzy rules to achieve precise positioning.

(5) Extension of Fuzzy Rules

The output u(t) of the fuzzy PID controller can be expressed in the basic form of PID control, that is[13]:

$$u(t) = K_P e(t) + K_I \int_0^t e(t)dt + K_D \frac{de(t)}{dt} \tag{12}$$

Here, u(t) is represented in the basic form of PID control.

e(t) denotes the deviation at the current moment, which is the difference between the target position and the actual position.

K_P is the proportional coefficient; K_I is the integral coefficient; K_D is the derivative coefficient. These three coefficients are dynamically adjusted based on the results of fuzzy inference.

The fuzzy inference process involves taking the deviation and its rate of change as inputs, mapping them to fuzzy subsets, calculating membership degrees, and then obtaining parameter adjustment amounts through rule-based inference. These adjustment amounts are added to the original PID parameters to yield new parameter values, which are used to calculate the control output. The core of the algorithm is to fuzzify the input variables through a fuzzy inference engine and, based on a fuzzy rule base, infer online adjustment values for the three key parameters (K_P, K_I and K_D) of the PID controller to meet different control performance requirements[14]. For different size categories of film-applying objects, differentiated control rules are formulated(as shown in Table 4).

Table 4

Differentiated Control Rules

Rule ID (Size Category)	ΔK_P	ΔK_I	ΔK_D
1 (>8″)	+20%	−10%	+15%
2 (<8″)	−15%	+5%	−10%

This dynamic adjustment control strategy addresses uncertainties and nonlinear factors during the film-applying process, ensuring a high degree of coincidence in the center positions and enhancing the quality and reliability of film application. It enables precise grasping and positioning of full-size screen protectors using only a single suction cup.

6. Prototype Experiment and Analysis

After the completion of the automatic film applying machine's design and subsequent debugging, it was successfully integrated into the actual production line, where it operated smoothly and met the anticipated design requirements. The machine has proven capable of fulfilling the practical demands of production. A physical representation of the machine is illustrated in Figure 21.

Fig. 21 Film-applying machine

The comparative experimental results between the fully automatic mobile phone film applying machine and manual film application are presented in Table5.

Table 5

Comparison of Work Efficiency between Manual and Machine Film Application

group	productivity (units per person per hour)	pass rate (%)
manual film application	19	75
machine film application	118	92

An analysis of Table 4 reveals that the productivity of automated film application is approximately six times that of manual film application, with a pass rate exceeding 90%, thus meeting the expected design requirements. A comparison of work efficiency is illustrated in Figure 22.

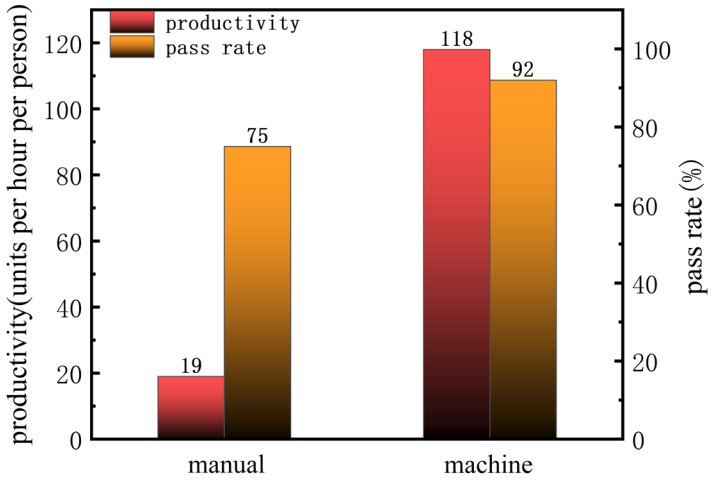

Fig. 22 A Comparison of Work Efficiency Between Manual Labor and Machine Operation

7. Conclusions

This study addresses the key challenge in the current market where mobile phone screen protector application relies heavily on manual operation, resulting in low efficiency. Based on the research findings, the following conclusions are drawn:

1.An automatic mobile phone screen protector application device has been designed. It accomplishes a series of technological actions, from screen protector positioning to adhesion. The device primarily consists of components such as a wiping mechanism, a base plate, and a structural frame, enabling functions like cleaning, suction, and screen protector application.

2.Simulation analysis indicates that the thickness of the base plate can be reduced by 10 mm. Given that the stress borne by the base plate is significantly lower than the material's yield strength, a hollow or porous structural design can be adopted to further reduce the component's weight. When the same constraints and load conditions are applied to the modified model, the calculated maximum deformation is 2.00×10^{-7} mm, and the maximum stress is 0.00110 MPa, which meet the design requirements. This not only reduces overall material consumption but also enhances structural reliability.

3.Prototype experiments demonstrate that the productivity of the automatic screen protector application is approximately six times that of manual operation, with a qualification rate exceeding 90%. Both productivity and qualification rate surpass those of manual methods, providing corresponding technical support and references for the mass production of the device.

REFERENCES

[1]. *Yuan, G., et al*., Human-robot collaborative disassembly in Industry 5.0: A systematic literature review and future research agenda. Journal of Manufacturing Systems, 2025. 79: p. 199-216.
[2]. *Wang, T., Y. Tao and H. Liu,* Current Researches and Future Development Trend of Intelligent Robot: A Review. International Journal of Automation and Computing, 2018. 15(5): p. 525-546.
[3]. *Fathi, M., et al.,* Balancing assembly lines with industrial and collaborative robots: Current trends and future research directions. Computers and Industrial Engineering, 2024. 193.
[4]. *Hui, J., Y. Li and J. Li,* experimental analysis and control of whitish inducement at corner of blunt trailing edge of fan blade. UPB Scientific Bulletin, Series D: Mechanical Engineering, 2023. 85(1): p. 59-74.
[5]. *Chunhai, Y. and D. Zhonghua,* mechanical properties research on a new auxiliary propulsion device of large slope roadheader. UPB Scientific Bulletin, Series D: Mechanical Engineering, 2025. 87(1): p. 3-18.
[6]. *Norton, R.L*., Machine design. 2006.
[7]. *Billieux, J.,* Problematic Use of the Mobile Phone: A Literature Review and a Pathways Model. Current Psychiatry Reviews, 2012. 8(4): p. -.
[8]. *Xu, T., R. Zhang and X. Si*, Effects of fluid dynamics Parameters on flow-accelerated corrosion at elbow of carbon steel pipeline. 2024.
[9]. *Atikoglu, B., et al.*, Workload analysis of a large-scale key-value store. ACM SIGMETRICS Performance Evaluation Review, 2012. 40(1).
[10]. R*oos, F., H. Johansson and J. Wikander*, Optimal selection of motor and gearhead in mechatronic applications. Mechatronics, 2006. 16(1): p. 63-72.
[11]. *Bartheld, R.G., et al*., Motor selection. 2004.
[12] S*on, Wonkyeong , et al.* "Stretchable Micro-Wrinkled Carbon Nanotube-Assembled Skin-Adhesive Patches with Suction-Cup Patterns for Human Breath-Derived Moisture Energy Harvesting." ACS nano 22(2025):19.
[13] *O'Dwyer, A.* . Handbook of PI and PID controller tuning rules, 2nd Edition. 2006.
[14] *Malashenko, Yu. E. , and I. A. Nazarova* . "Differentiated Estimates of a Multiuser Network in the Case of Node Damage." Journal of Computer and Systems Sciences International (2025).